Proton Spectra with Low-Energy-Threshold from 40- and 70-MeV Proton-Induced Reactions

Yuji YAMAGUCHI[1], Toshiya SANAMI[2], Yusuke KOBA[3] and Yusuke UOZUMI[1]

[1]Department of Applied Quantum Physics and Nuclear Engineering, Kyushu University

744 Motooka, Nishi-ku, Fukuoka-shi, Fukuoka-ken 819-0395 Japan

[2]High Energy Accelerator Research Organization

1-1 Oho, Tsukuba-shi, Ibaraki-ken 305-0801 Japan

[3]National Institute for Quantum and Radiological Science and Technology

4-9-1 Anagawa, Inage-ku, Chiba-shi, Chiba-ken 263-8555 Japan

e-mail: yyamaguchi@nucl.kyushu-u.ac.jp

We have developed a low-energy-threshold detector consisting of a Bragg curve counter (BCC), two silicon-surface barrier detectors and a bismuth germanate scintillator to obtain experimental double-differential cross section (DDX) data on (p, p'x) reactions for incident energies of several tens of MeV. The BCC can identify particles by itself and can do so for protons down to 1 MeV. The developed detector is used to measure proton spectra for incident energies of 40 and 70 MeV at $60 - 150°$. The minimum energy in the spectrum data is 1.3 MeV, which gives spectra in the whole energy range. Measured spectra are compared with calculation results of intranuclear cascade plus evaporation models and nuclear data library.

1. Introduction

Energy and angular distributions of secondary particles from energetic proton-nucleus reactions are required to estimate the spatial distributions of energy deposition and radiation damage for the engineering design of an accelerator driven system and a particle radiation therapy facility. Because the estimation is performed using a Monte Carlo simulation code such as PHITS [1], the nuclear reaction models must have high predictive power for energy and angular distributions. A two-stage model, which consists of an intranuclear cascade (INC) model [2, 3] and an evaporation model [4, 5], is generally used to describe the emission of secondary particles from proton-nucleus reactions up to several hundreds of MeV. In recent studies [6, 7], the INC model followed by the generalized evaporation model (GEM) has been improved for (p, p'x) reactions on light-to-heavy targets below 100 MeV. According to Ref. [7], the calculation results of the INC model covering high-energy range mainly above 10 MeV reproduce the energy and angular distributions of experimental data for targets from ^{12}C to ^{209}Bi at angles between 15°

and 130°, but the GEM results covering low-energy range mainly below 10 MeV show discrepancies for heavy targets ($A \geq 120$). To improve the GEM, systematic experimental data covering low-energy range for (p, p'x) reactions are required for not only heavy targets but also light and medium targets at various angles from forward to backward.

Bertrand et al. [8] and Harada et al. [9] have reported experimental data on light-to-heavy targets for incident proton energy $E_p < 100$ MeV. Bertrand et al. obtained proton spectra for $E_p = 29$, 39, and 62 MeV, while Harada et al. obtained spectra for $E_p = 42$ and 68 MeV. However, the spectra on a ^{197}Au target exhibit different tendencies around 55° and 120° in the secondary energy range of $2 - 6$ MeV between the data for $E_p \sim 65$ MeV. In addition, both sets of data are insufficient below 10 MeV for $E_p \sim 40$ MeV. The discrepancy at $2 - 6$ MeV should be investigated and insufficient coverage of spectra for $E_p \sim 40$ MeV should be updated for improvement of the GEM. Thus, new experimental data of (p, p'x) reactions are desired for secondary energies down to 2 MeV for $E_p = 40$ and 70 MeV.

In this study, we measure the data which satisfy the requirement above. For the measurement, we develop a low-energy-threshold detector consisting of a Bragg curve counter (BCC) [10], two silicon-surface barrier detectors (SSDs) and a bismuth germanate (BGO) scintillator.

2. Experiment

The experiment was performed at cyclotron facility of National Institute of Radiological Sciences. The experimental setup and the low-energy-threshold detector are described in detail in Ref. [11]. Outlines of the setup and the detector are described herein. The plan view of the experimental setup is shown in Fig. 1. A scattering chamber was connected directly to the beam duct of the cyclotron and evacuated to less than 10^{-3} Pa. Incident protons hit a thin-film target located inside the scattering chamber and entered a Faraday cup consisting of a stainless–steel pipe and a graphite beam dump. The targets for ^{nat}C, ^{27}Al, ^{nat}Cu, ^{nat}Ag, ^{nat}Ta, and ^{197}Au were mounted on a target changer. Thicknesses of 11, 5, 3, 3, 3, and 0.5 μm were chosen for polyethylene, aluminum, copper, silver, tantalum, and gold foils, respectively. For the ^{nat}C target, a 134-μm-thick graphite foil was also used to remove the proton component scattered by hydrogen in the polyethylene. Energy spectra of secondary particles emitted from the target were measured at 60°, 120°, and 150° in the laboratory system using the low-energy-threshold detector.

The schematic drawing of the low-energy-threshold detector is shown in Fig. 2. This detector consists of a BCC, two SSDs, and a BGO scintillator. The BCC is a parallel-plate gas ionization chamber with a grid. The BCC can determine the energy E_{BCC} and the atomic number of a low-energy charged particle from the integral and peak height, respectively, of the anode signal, which reflects the charge distribution along the trajectory of the charged particle [14]. The Ar + 10 % CH$_4$ counting gas is kept inside the cylindrically shaped chamber using O-rings. The electrodes of the BCC consist of a cathode, nine field shaping rings, a grid, and an anode. The distances from the cathode to the grid and from the grid to the anode are set to 150 mm and 5 mm, respectively. The cathode is a stainless-steel disk with a central hole 10 mm in diameter covered with a 2.2-μm-thick aluminized Mylar film. Because the aluminized

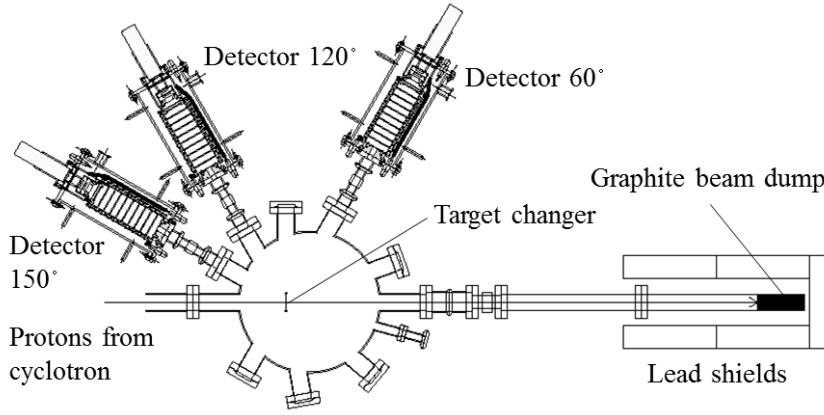**Figure 1.** Plan view of experimental setup. Incident protons come from the left side of this view.

Figure 2. Schematic drawing of low-energy-threshold detector. Secondary particles come from the left side of this drawing and pass through the entrance window.

surface and the stainless-steel disk are connected electrically, the cathode plays the role of a thin entrance window that admits secondary charged particles with small energy loss. The field shaping rings and the grid are arranged at equal intervals and connected with a chain of 1-MΩ resistors to maintain a uniform electric field. The anode plate is a stainless-steel disk with a central hole 32 mm in diameter and covered with a 5.7-μm-thick aluminum foil. Thus, the anode enables energetic secondary particles to penetrate with small energy loss. The energetic particles are identified using $\Delta E - E$ method with the BCC and rear detectors. In this case, the BCC works as a transmission detector.
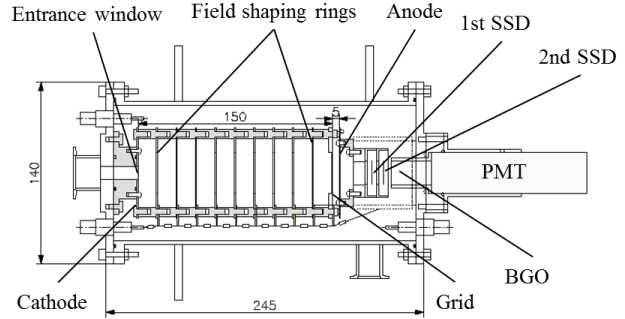
The measured data were corrected to remove the effects of background component using data obtained without a target. The energy losses in the target, entrance window, and anode were compensated for by shifting the energy scale by calculation using the SRIM code [12]. Finally, DDXs were obtained by

$$\frac{\mathrm{d}^2\sigma}{\mathrm{d}\Omega \mathrm{d}E} = \frac{Y(E)}{s\phi\Delta\Omega\Delta E},\qquad(1)$$

where $Y(E)$ is the number of charged particles, s is the number of target atoms per unit area, ϕ is the number of incident protons, $\Delta\Omega$ is the solid angle, and ΔE is the energy bin width. The solid angle $\Delta\Omega$ was determined experimentally by α-particle counting using a [241]Am check source placed instead of the target.

3. Results and discussion

Figure 3 shows the plot of E_{BCC} versus Bragg peak height (atomic number) obtained using 53.3 kPa counting gas. In this figure, hydrogen and helium isotopes are identified. On the high-energy side,

those particles that penetrated the anode are observed within dashed circles. In the energy range from 1 MeV to 3 MeV, the hydrogen isotopes of protons, deuterons and tritons are clearly identified because the Bragg peak is characterized by the mass number of the charged particle besides the atomic number. Protons down to 1.1 MeV are separated from other particles in Fig. 3. Thus, the threshold energy of 1.1 MeV was achieved for proton identification.

Figure 4 shows the plot of ΔE (BCC) versus E (first SSD) obtained using 53.3 kPa counting gas. The hydrogen isotopes are also identified in this figure because of the satisfactory energy resolution of the BCC. Although the identified proton line overlaps partially with the folding-back lines of the hydrogen isotopes that penetrated the first SSD, the penetrating events can be removed using the signal of the second SSD in offline analysis.

Figure 5 shows proton spectra for 40- and 70-MeV incident protons on ^{nat}C, ^{27}Al, ^{nat}Cu, ^{nat}Ag, ^{nat}Ta, and ^{197}Au targets at $60 - 150°$. The measured spectra were obtained in a wide energy range. The minimum energy of the measured data is 1.3 MeV, which is 0.2 MeV above the particle identification threshold because of compensating for the energy losses in the target foil and the entrance window. In comparison of the ^{nat}Cu(p, p'x) spectra with the ^{nat}Ta(p, p'x) spectra below 10 MeV for $E_p = 70$ MeV, the ^{nat}Cu(p, p'x) spectra show a broad peak whereas the ^{nat}Ta(p, p'x) spectra show monotonic decrease as the proton energy decreases, which reflects the difference in the Coulomb barrier. This target dependence is also observed in comparison of ^{nat}Ag(p, p'x) spectra with the ^{197}Au(p, p'x) spectra for $E_p = 40$ MeV.

Calculation results reproduce measured spectra for ^{nat}C, ^{27}Al and ^{nat}Cu targets below 10 MeV. However, calculations disagree with measured spectra for heavy targets as follows. The INC plus GEM results and JENDL-4.0/HE results overestimate measured ^{nat}Ta(p, p'x) spectra for $E_p = 70$ MeV. The ^{197}Au(p, p'x) spectra of the INC plus GEM have a threshold at 6 MeV for $E_p = 40$ MeV whereas there are measured data below 6 MeV.
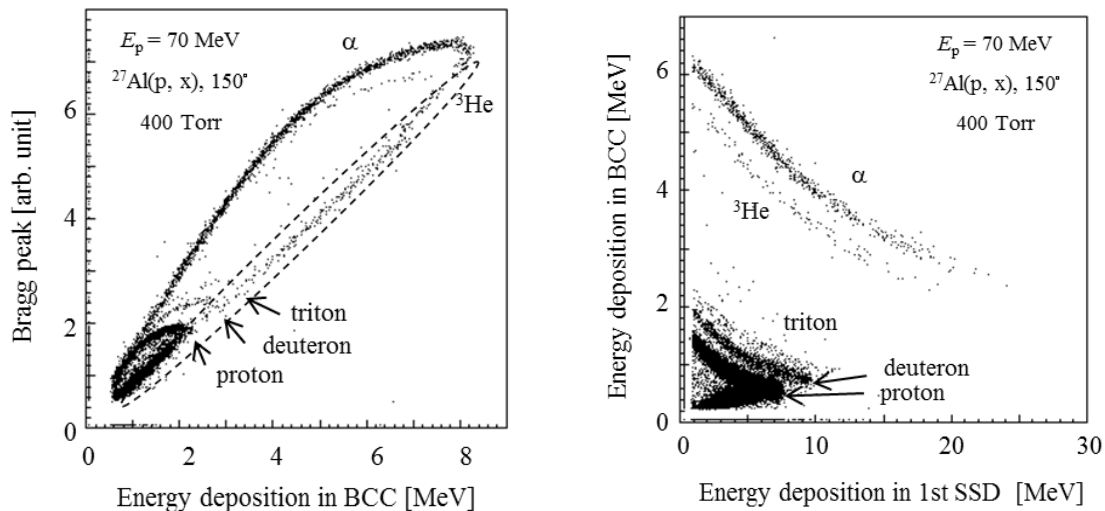

Figure 3. Plot of E_{BCC} versus Bragg peak height. The particles identified as proton, deuteron, triton, ^{3}He and α are shown.

Figure 4. Plot of ΔE (BCC) versus E (first SSD). The particles identified as proton, deuteron, triton, ^{3}He and α are shown.
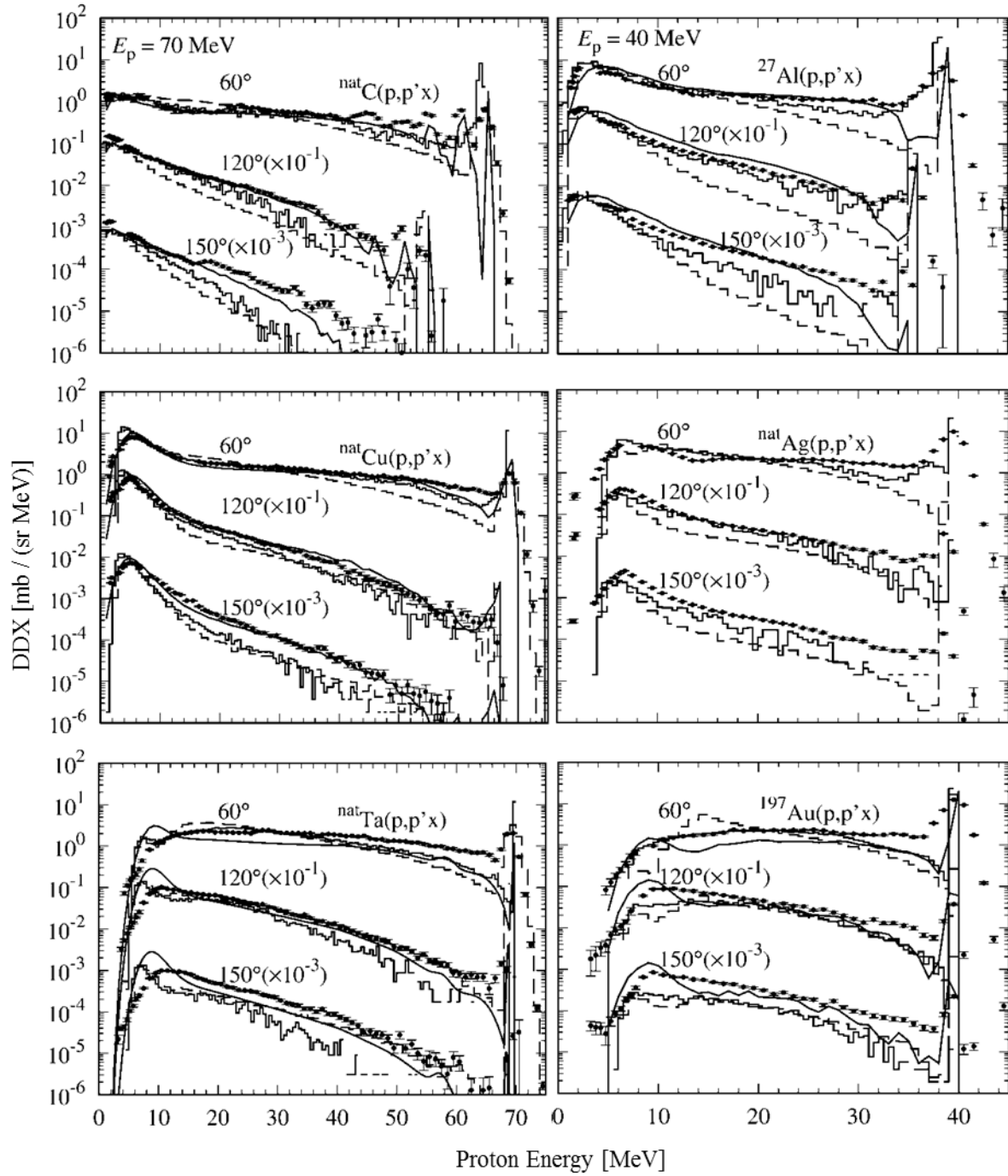
Figure 5. Measured and calculated proton spectra for 40- and 70-MeV incident protons on ^{nat}C, ^{27}Al, ^{nat}Cu, ^{nat}Ag, ^{nat}Ta, and ^{197}Au targets at $60 - 150°$. Measured spectra are shown using closed circles with bar indicating statistical uncertainties. Calculation results of JENDL-4.0/HE, INC plus GEM in Ref. [7] and INC plus GEM used in PHITS as the default model [2] are shown with smooth curves, solid histograms and dashed histograms, respectively.

4. Conclusion

We developed a low-energy-threshold detector consisting of a BCC, two SSDs, and a BGO

scintillator to obtain experimental data on (p, p'x) reactions covering the low-energy range. We used the detector and obtained proton spectra down to 1.3 MeV at 60 – 150° for targets of ^{nat}C, ^{27}Al, ^{nat}Cu, ^{nat}Ag, ^{nat}Ta, and ^{197}Au using 40- and 70-MeV protons. The resultant spectra were compared with results of the INC plus GEM and JENDL-4.0/HE. Below 10 MeV, calculation results reproduced measured spectra for ^{nat}C, ^{27}Al and ^{nat}Cu targets. For the ^{nat}Ta target, calculations overestimated measured spectra.

References

[1] T. Sato, Y. Iwamoto, S. Hashimoto, et al. Features of particle and heavy ion transport code system (PHITS) version 3.02. J. Nucl. Sci. Technol. 2018;55(6):684-690.

[2] A. Boudard, J. Cugnon, J. C. David, et al. New potentialities of the Liege intranuclear cascade model for reactions induced by nucleons and light charged particles. Phys. Rev. C 2013;87:014606.

[3] Y. Sawada, Y. Uozumi, S. Nogamine, et al. Intranuclear cascade with emission of light fragment code implemented in the transport code system PHITS. Nucl. Instrum. Methods Phys. Res. B 2012;291:38-44.

[4] S. Furihata, T. Nakamura. Calculation of nuclide productions from proton induced reactions on heavy targets with INC/GEM. J. Nucl. Sci. Technol. 2002;39(2):758-761.

[5] J. Benlliure, A. Grewe, M. de Jong, et al. Calculated nuclide production yields in relativistic collisions of fissile nuclei. Nucl. Phys. A 1998;628:458-478.

[6] Y. Uozumi, T. Yamada, S. Nogamine, et al. Intranuclear cascade model including collective excitations and trajectory deflections for (p, p'x) reactions around 50 MeV. Phys. Rev. C 2012;86:034610.

[7] Y. Uozumi, T. Yamada, M. Nakano. Intranuclear cascade model for 50-MeV-region (p, p'x) reactions over a wide target mass range. J. Nucl. Sci. Technol. 2015;52(2):264-273.

[8] F. E. Bertrand, R. W. Peelle. Complete hydrogen and helium particle spectra from 30- to 60-MeV proton bombardment of nuclei with A = 12 to 209 and comparison with the intranuclear cascade model. Phys. Rev. C 1973;8:1045-1064.

[9] M. Harada, Y. Watanabe, Y. Tanaka, et al. Light charged-particle production in proton-induced reactions on ^{12}C, ^{27}Al, ^{58}Ni, ^{90}Zr, ^{197}Au, and ^{209}Bi at 42 and 68 MeV. J. Nucl. Sci. Technol. 2002;39(2):393-396.

[10] T. Sanami, M. Hagiwara, T. Oishi, et al. A Bragg curve counter with an active cathode to improve the energy threshold in fragment measurements. Nucl. Instrum. Methods Phys. Res. A 2008;589:193-201.

[11] Y. Yamaguchi, T. Sanami, Y. Koba, et al. Low-energy-threshold detector for measuring proton spectra at several tens of MeV using Bragg curve spectroscopy. Nucl. Instrum. Methods Phys. Res. A 2020;953:163158.

[12] J. F. Ziegler, M. D. Ziegler, J. P. Biersack. SRIM – The stopping and range of ions in matter (2010). Nucl. Instrum. Methods Phys. Res. B 2010;268:1818-1823.